Conference materials
UDC 523.985.3
DOI: https://doi.org/10.18721/JPM.161.274

Electron acceleration in models with a vertical current sheet

A.N. Shabalin✉, Yu.E. Charikov

Ioffe Institute, St. Petersburg, Russia

✉ ShabalinAN@mail.ioffe.ru

Abstract. Model of solar flares with a vertical current sheet and a cusp above the magnetic arcade is considered. In some flares, such magnetic field geometry can be observed directly in the extreme ultraviolet range. According to the model, the relaxation of helmet-like magnetic loops formed due to magnetic field reconnection is supposed. During the relaxation, the magnetic field and the loop length vary with time. Consequently, a betatron acceleration and first-order Fermi electron acceleration appeared. In a kinetic approach the time-dependent kinetic equation for the distribution function of initially accelerated electrons is numerically solved. It is shown that because of such acceleration, the electron energy spectra changes significantly. The proportion of high-energy electrons with energies of more than 200 keV increases by 1–3 orders of magnitude depending on the pitch-angular distribution of accelerated electrons formed in the primary accelerator – the current sheet.

Keywords: solar flare, acceleration, magnetic reconnection_

Citation: Shabalin A.N., Charikov Yu.E., Electron acceleration in models with a vertical current sheet, St. Petersburg State Polytechnical University Journal. Physics and Mathematics. 16 (1.2) (2023) 485–491. DOI: https://doi.org/10.18721/JPM.161.274

Материалы конференции
УДК 523.985.3
DOI: https://doi.org/10.18721/JPM.161.274

Ускорение электронов в моделях с вертикальным токовым слоем

А.Н. Шабалин✉, Ю.Е. Чариков

Физико-Технический институт им. А.Ф. Иоффе, РАН, Санкт-Петербург, Россия

✉ ShabalinAN@mail.ioffe.ru

Аннотация. Модели солнечных вспышек с вертикальным токовым слоем и каспом в области над аркадой замкнутых магнитных петель часто привлекаются при анализе вспышечных событий. В некоторых событиях подобную конфигурацию удается наблюдать непосредственно, в крайнем ультрафиолетовом диапазоне. В подобной геометрии магнитных полей рассматривается процесс релаксации вновь образуемых, после магнитного пересоединения, замкнутых магнитных петель и возникающее, как следствие, вторичное ускорение электронов за счет бетатронного ускорения и ускорения Ферми первого рода. В результате решения нестационарного кинетического уравнения для первично ускоренных электронов показано, что в результате процесса доускорения существенно изменяются со временем их энергетические спектры. Доля высокоэнергичных электронов с энергиями более 200 кэВ возрастает на 1–3 порядка в зависимости от питч-углового распределения ускоренных электронов, сформированного в первичном ускорителе — токовом слое.

Ключевые слова: солнечная вспышка, ускорение, магнитное пересоединение_

Ссылка при цитировании: Шабалин А.Н., Чариков Ю.Е. Ускорение электронов в моделях с вертикальным токовым слоем // Научно-технические ведомости СПбГПУ. Физико-математические науки. 2023. Т. 1.2 № .16. С. 485–491. DOI: https://doi.org/10.18721/JPM.161.274

Introduction

According to observations and modeling, configurations of magnetic fields with a vertical current sheet and sources on the photosphere are possible in active regions of the atmospheres of flaring stars, in particular the Sun [1–3]. Relaxation of the magnetic structure initially extended in the direction of the current sheet to a closed configuration similar to a dipole is accompanied by a longitudinally - transverse contraction of the magnetic loop. It leads to betatron acceleration and first-order Fermi acceleration [4–6]. The peculiarity of these processes is the angular anisotropy of the energy gained by electrons. Betatron acceleration leads to acceleration in the transverse direction. First-order Fermi acceleration increases the longitudinal component of the particle velocity.

Observational signs of magnetic loops relaxation include, for example, separation of coronal X-ray sources at different energies in height, as well as a decrease in their height with time in the initial phase of the flare [7, 8]. According to the model concepts [9], current sheets have small spatial thicknesses and, therefore, are difficult to observe, especially in the X-ray range. Nevertheless, data at various wavelengths indicate their existence [2, 10–12].

The rate of energy gain by an electron due to the betatron and Fermi acceleration is easily obtained from the conservation of the first (transverse) and the second (longitudinal) adiabatic invariants in a magnetic field. The relative rate of increase of the transverse energy is ~ $(1-\mu^2)$ $d\ln B/dt$, and the longitudinal one is ~ $\mu^2 d\ln L/dt$, where $\mu = \cos(\alpha)$, α is the pitch angle of an electron, $B(t)$ is the magnetic field, $L(t)$ is the length of the loop. Thus, the acceleration depends on the rate of the magnetic field change in the loop during relaxation. In the work within the framework of solving the kinetic equation for the distribution function of accelerated electrons, the calculation of additional (secondary) acceleration of electrons due to the mechanisms of betatron and Fermi acceleration is carried out.

The modeling of collapsing traps

To solve the problem of additional electron acceleration, we will perform modeling of the kinetics of accelerated electrons in a relaxing magnetic field with a cusp structure. We will consider a time-dependent one-dimensional Fokker–Planck type equation with a model nonstationary magnetic field and a time-variable plasma density along the flare loop. The kinetic equation is considered in detail in [13]. The Fokker-Planck equation can be written in the form [14–17]

$$\frac{\partial f}{\partial t} = -\beta c\mu\frac{\partial f}{\partial s} + \beta c\frac{\partial \ln B}{\partial s}\frac{\partial}{\partial \mu}\left[\frac{(1-\mu^2)}{2}f\right] + C_1\frac{c}{\lambda_0}\frac{\partial}{\partial E}\left(\frac{f}{\beta}\right) + C_2\frac{c}{\lambda_0\beta^3\gamma^2}\frac{\partial}{\partial \mu}\left[(1-\mu^2)\frac{\partial f}{\partial \mu}\right] + \\ + \frac{eY\beta\mu}{m_e c}\frac{\partial f}{\partial E} + \frac{eY}{m_e\beta c}\frac{\partial}{\partial \mu}\left[(1-\mu^2)f\right] + \frac{\partial(\dot{E}f)}{\partial E} + \frac{\partial(\dot{\mu}f)}{\partial \mu} + S(E,\mu,s,t), \quad (1)$$

where $f(E,\mu,s,t)$ is the non-thermal electron distribution function which is defined so that the integrals over variables E, μ, s yield the linear density [18], s is the distance along the magnetic field line ($s = 0$ corresponds to the loop top), t is the time, $\mu = \cos(\alpha)$ is the cosine of the pitch angle, $\lambda_0(s) = 10^{24}/n(s)\ln\Lambda$, $n(s)$ is the plasma density; $\Lambda = \frac{3k_B T_e}{2e^2}\left(\frac{k_B T_e}{8\pi e^2 n}\right)^{0.5}$ [19], k_B is the Boltzmann constant, T_e is electron temperature, e is electron charge, $\beta = v/c$, v is non-thermal

electron speed, c is speed of light, m_e is electron mass, $\gamma = E+1$ is Lorentz factor of the electron, E is the kinetic energy of an electron, expressed in units of the electron rest mass energy, $\tilde{N}_1 = x + \frac{1-x}{2}\frac{\ln \beta^2 g^2 E/\alpha_F^4}{\ln \Lambda}$, $C_2 = \frac{1}{2} + \frac{1+g}{4} C_1$ [20, 21] are the coefficients taking into account the contribution of partially ionized plasma to the energy loss and angular scattering of fast electrons, α^4_F is fine structure constant, x is fraction of ionized hydrogen atoms, $g \sim 1$. The influence of betatron and Fermi processes on the energy and pitch-angles described by the partial derivatives (two terms at the last line of Eq. 1). These terms are considered in more detail in the work [13].

We assume that many episodes of energy release and subsequent "collapses" of magnetic structures occur in the region of the current sheet. However, in this work, we consider the relaxation of one magnetic structure in order to analyze the effects of accumulation of accelerated electrons in a single loop. The collapse times in the range 10–60 s correspond to the possible relaxation times of magnetic loops at sub-Alfven velocities. The paper shows the results for the first 6 seconds, because with a selected collapse time of about 8–10 seconds, the acceleration efficiency is maximum in the initial 6 seconds.

The magnitude of the magnetic field induction at the looptop varied from 20 G to ~200 G. Due to the conservation of the magnetic flux and the number of particles inside the closed magnetic loop, the cross-sectional area of the loop and the plasma density along the loop variates following the change in the magnetic field.

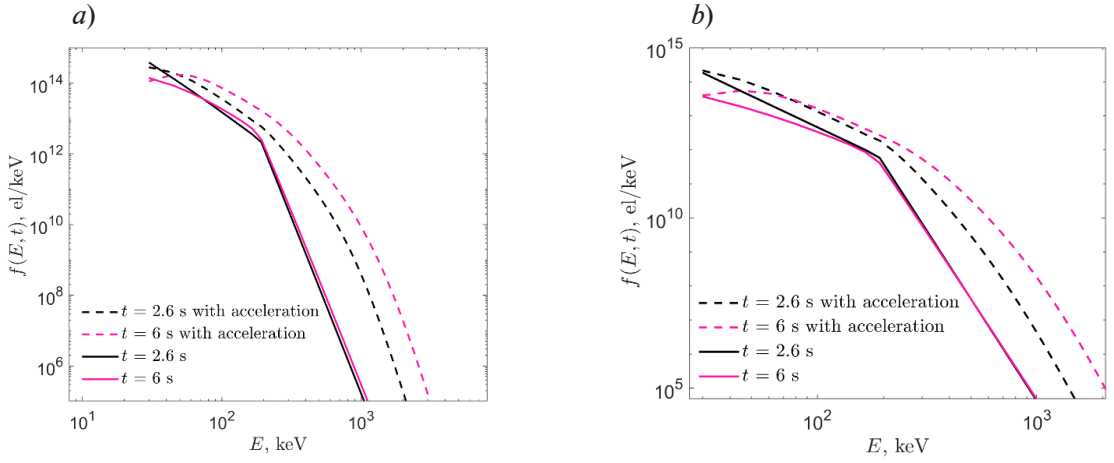

Fig. 1. Looptop energy spectra of accelerated electrons. Left panel: the spectra for the isotropic model S(α) = 1. Right panel: for the anisotropic model $S(\alpha) = \cos^{12}(\alpha)$. The curves are given for two time instants: the injection peak phase at t = 2.6 s and the decay phase at t = 6 s. The spectrum exponents of injected electrons in the models are δ = 3

Thus, at the beginning of the magnetic field relaxation process, the closed loop was an effective trap with a large magnetic ratio of $B_{max}/B_0 = 80$ (20 G at the top and 1.6 kG at the footpoints) for injected electrons accelerated in the current sheet. During the collapse of the magnetic field, the loss cone increases, the plasma density in the coronal part of the loop increases, leading to an increase of Coulomb scattering of accelerated electrons and the effective precipitation of electrons into the chromosphere. In the model the final number density and energy spectrum of accelerated electrons significantly depend on several physical processes – the rate of change of the magnetic field, the Coulomb scattering, the effects of return current, magnetic mirroring, plasma and magnetic field parameters, the pitch angular distribution of accelerated electrons at the injection time.

We consider the effect of betatron and Fermi acceleration on the spectra of accelerated electrons. The rate of energy gain by an accelerated electron during betatron acceleration is determined by the term $\sim(1-\mu^2)d\ln B/dt$ in the kinetic equation, and the term $\sim\mu^2 d\ln L/dt$ determines the efficiency of first-order Fermi acceleration. As can be seen, the pitch--angular dependence of the rate of energy gain in these processes is sharply different: transverse acceleration in betatron acceleration and longitudinal acceleration in the Fermi mechanism.

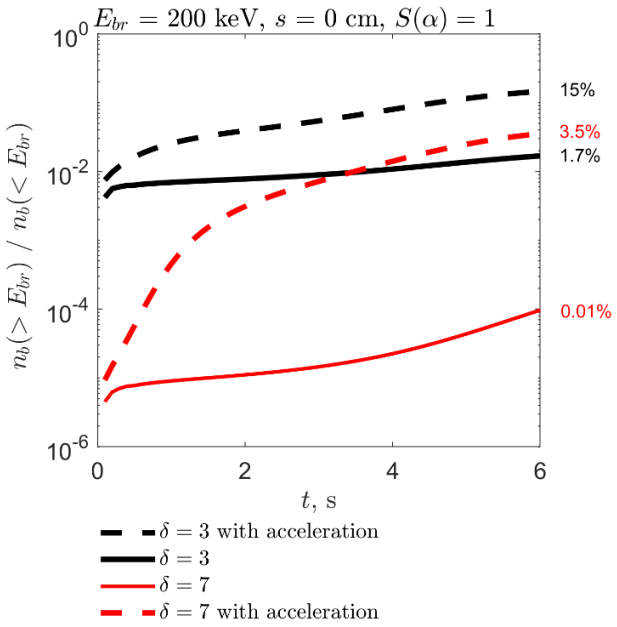

Fig. 2. The dynamics over time of the ratio of the number density of electrons with energy $E > E_{br}$ to electrons with $E < E_{br}$, E_{br} = 200 keV. The ratios are given for the looptop. The pitch-angular distribution of electrons at the injection site is isotropic

The results for two models of accelerated electrons injection into the top of a magnetic loop will be presented below for isotropic model S(α) = 1 and anisotropic one S(α) = $\cos^{12}(\alpha)$. Suppose that at the injection site the energy spectrum is broken power-law with spectrum exponents δ = 3 or 7 in the energy range of 30–200 keV and δ = 10 in the energy range of 200 keV – 10 MeV. The choice of the break point in the spectrum is due to the fact that it is supposed to analyze the efficiency of increasing the number of accelerated electrons with energies that make a predominant contribution to the gyrosynchrotron radiation in the 17–34 GHz range, namely, with energies > 200 keV. The hardness of the emission spectra in the hard X-ray range during flares varies over a wide range. Therefore, variants of the initial soft δ = 7 and hard δ = 3 electron spectra are considered. The angular distribution of accelerated electrons at the moment of injection into the collapsing loop is not known, therefore we considered the limiting cases of isotropic S(α) = 1 and strongly anisotropic S(α) = $\cos^{12}(\alpha)$ distributions of accelerated electrons at the moment of injection.

The initial plasma density at the looptop was set to $7 \cdot 10^8$ cm^{-3} [22, 23]. In the chromosphere, the calculations are performed using height density distribution corresponding to hydrostatic equilibrium [24]. The maximum plasma density at footpoints in the models is $3 \cdot 10^{13}$ cm^{-3}. To compare the results, a model with a stationary magnetic field and plasma density at the top of the loop of 10^{10} cm^{-3} is also considered.

Fig. 1 shows the spectra of accelerated electrons for a model with permanent distributions of the magnetic field and plasma density (solid curves, hereinafter referred to as the stationary model (S-model)) and a model with longitudinal-transverse compression of the magnetic loop (dashed curves, hereinafter referred to as the non-stationary model (NS-model)). The energy injected by accelerated electrons in both models is $2 \cdot 10^9$ erg cm^{-2}s^{-1} for a time period of 6 s. The figure shows that the dashed curves in the NS-model exceed the solid curves of the S-model in the energy range of ~ 45 keV – 8 MeV, which is caused by energy gain due to betatron and Fermi accelerations.

In the range of 30–45 keV, the dashed curves are below the solid curves. This decrease in the number of electrons is explained by more efficient energy losses due to Coulomb interactions with plasma protons, as well as the result of acceleration processes i.e. spectral energy transfer. The spectral energy transfer results in the energy break in the electron injection spectrum in the 200 keV disappears.

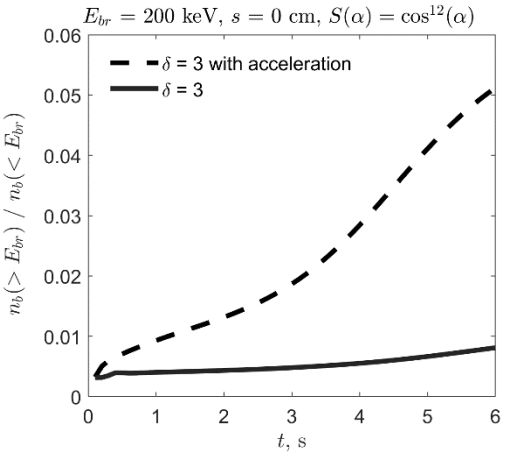

Fig. 3. Same as in Fig. 2 for anisotropic injection of accelerated electrons

The analysis of the observed hard X-ray radiation in the energy range >200 keV by modern spectrometers causes difficulties arising from a sharp decrease in the number of X-ray quanta. Nevertheless, the spectra of high-energy electrons with energies >200 keV determine the gyrosynchrotron radiation at frequencies of ~8–40 GHz [25, 26]. In this regard, let us consider the time dependence of the fraction of electrons accelerated above the energy E_{br} = 200 keV relative to electrons of lower energies. Above-mentioned ratios are shown in Fig. 2 for the isotropic model and in Fig. 3 for the anisotropic model. As in Fig. 1, the dashed curves correspond to the NS-model. The red curves were obtained in a model with a soft electron energy spectrum $\delta = 7$ at the time of injection, and the black curves were obtained in a model with a hard spectrum $\delta = 3$. Figs. 2 and 3 show that the dashed curves significantly exceed the solid curves already starting from the first second from the beginning of injection. At the time $t = 6$ s for the isotropic electron injection with spectrum exponent $\delta = 7$ (Fig. 2) in the NS-model, the proportion of high-energy electrons is 350 times greater than in the S-model. In the case of the injection with a hard spectrum $\delta = 3$, the proportion of high-energy electrons in the NS-model is 5–10 times greater.

Thus, in a model with a vertical current sheet, the proportion of accelerated electrons above the E_{br} energy in a relaxing magnetic field could lead to an increase in hard X-ray, gamma radiation and radio emission at frequencies of 8–40 GHz. We also note that in the analyzed models, according to [13], the additional acceleration of electrons is associated with a higher efficiency of the betatron mechanism in comparison with the first order Fermi acceleration.

Conclusion

The paper analyzes the efficiency of secondary acceleration of electrons to MeV energies, previously accelerated in a vertical current sheet to energies of hundreds of keV. For this purpose, a time-dependent kinetic equation was numerically solved for accelerated electrons in a magnetoactive plasma, whose parameters change over time as a result of the relaxation process of magnetic structures. The results of calculations show that the additional acceleration resulting from the relaxation of the magnetic field and the processes of betatron acceleration and first-order Fermi increases the proportion of high-energy electrons by 1–3 orders of magnitude. In absolute values, this makes it possible to increase the density of accelerated electrons with energies above 200 keV also by 1–3 orders of magnitude. If we assume that due to the primary acceleration, the number density of accelerated electrons with an energy >200 keV in the magnetic loop is of the order of 10^2–10^3 cm^{-3}, then the secondary acceleration considered in the article will lead to an increase in n_b (E>200 keV) to values of the order of 10^4–10^6 cm^{-3}. The number density of high-energy electrons ~10^5 cm^{-3} is already sufficient to register radiation in the radio band of 8–40 GHz [27]. Thus, the numerical results of electrons propagation in collapsing traps make it possible to significantly lower the requirements for acceleration of highenergy electrons in the primary accelerator — the current sheet.

REFERENCES

1. **Gary D.E.**, **Chen B.**, **Dennis B.R.**, **Fleishman G.D.**, **Hurford G.J.**, **Krucker S.**, **McTiernan J.M.**, **Nita G.M.**, **Shih A.Y.**, **White S.M.**, **Yu S.**, Microwave and Hard X-Ray Observations of the 2017 September 10 Solar Limb Flare, The Astrophysical Journal, 863 (1) (2018) 83.
2. **Warren H.P.**, **Brooks D.H.**, **Ugarte-Urra I.**, **Reep J.W.**, **Crump N.A.**, **Doschek G.A.**, Spectroscopic Observations of Current Sheet Formation and Evolution, The Astrophysical Journal, 854 (2) (2017) 122.
3. **Jiang C.**, **Zou P.**, **Feng X.**, **Hu Q.**, **Liu R.**, **Vemareddy P.**, **Duan A.**, **Zuo P.**, **Wang Y.**, **Wei F.**, Magnetohydrodynamic Simulation of the X9.3 Flare on 2017 September 6: Evolving Magnetic Topology, The Astrophysical Journal, 869 (1) (2018) 13.
4. **Somov B.V.**, **Kosugi T.**, Collisionless Reconnection and High-Energy Particle Acceleration in Solar Flares, The Astrophysical Journal, 485 (2) (1997) 859–868.
5. **Bogachev S.A.**, **Somov B. V.**, Acceleration of Charged Particles in Collapsing Magnetic Traps During Solar Flares, Astronomy Reports, 45 (2) (2001) 157–161.
6. **Karlicky M.**, **Barta M.**, X-Ray Loop-Top Source Generated by Processes in a Flare Collapsing Trap, The Astrophysical Journal, 647 (2) (2006) 1472–1479.
7. **Veronig A.M., Karlický M., Vršnak B., Temmer M., Magdalenić J., Dennis B.R., Otruba W., Pųtzi W.**, X-ray sources and magnetic reconnection in the X3.9 flare of 2003 November 3, Astronomy & Astrophysics, 446 (2) (2006) 675–690.
8. **Sui L., Holman G.D., Dennis B.R.**, Evidence for Magnetic Reconnection in Three Homologous Solar Flares Observed by RHESSI, The Astrophysical Journal, 612 (1) (2004) 546–556.
9. **Lin J., Forbes T.G.**, Effects of reconnection on the coronal mass ejection process, Journal of Geophysical Research: Space Physics, 105 (A2) (2000) 2375–2392.
10. **Webb D.F., Burkepile J., Forbes T.G., Riley P.**, Observational evidence of new current sheets trailing coronal mass ejections, Journal of Geophysical Research: Space Physics, 108 (A12) (2003) 1440.
11. **Sui L., Holman G.D.**, Evidence for the Formation of a Large-Scale Current Sheet in a Solar Flare, The Astrophysical Journal, 596 (2) (2003) L251–L254.
12. **Ko Y., Raymond J.C., Lin J., Lawrence G., Li J., Fludra A.**, Dynamical and Physical Properties of a Post–Coronal Mass Ejection Current Sheet, The Astrophysical Journal, 594 (2) (2003) 1068–1084.
13. **Shabalin A.N.**, **Charikov Y.E.**, **Sharykin I.N.**, Early-stage Coronal Hard X-Ray Source in Solar Flares in the Collapsing Trap Model, The Astrophysical Journal, 931 (27) (2022) 13.
14. **Hamilton R.J., Lu E.T., Petrosian V.**, Numerical solution of the time-dependent kinetic equation for electrons in magnetized plasma, The Astrophysical Journal, 354 (1990) 726–734.
15. **Zharkova V. V., Kuznetsov A.A., Siversky T. V.**, Diagnostics of energetic electrons with anisotropic distributions in solar flares. I. Hard X-rays bremsstrahlung emission, Astronomy and Astrophysics, 512 (2010) A8.
16. **Filatov L. V., Melnikov V.F., Gorbikov S.P.**, Dynamics of the spatial distribution of electrons and their gyrosynchrotron emission characteristics in a collapsing magnetic trap, Geomagnetism and Aeronomy, 53 (8) (2013) 1007–1012.
17. **Minoshima T., Masuda S., Miyoshi Y.**, Drift-kinetic modeling of particle acceleration and transport in solar flares, The Astrophysical Journal, 714 (1) (2010) 332–342.
18. **McClements K.G.**, The effects of magnetic field geometry on the confinement of energetic electrons in solar flares, Astronomy and Astrophysics, 253 (1992) 261–268.
19. **Ginzburg V.L.**, Theoretical physics and astrophysics. Additional chapters.V.L. Ginzburg.-Moscow:Nauka, (1981) 503 c.
20. **Leach J., Petrosian V.**, Impulsive phase of solar flares. I - Characteristics of high energy electrons , The Astrophysical Journal, 251 (1981) 781.
21. **Emslie A.G.**, The collisional interaction of a beam of charged particles with a hydrogen target of arbitrary ionization level, The Astrophysical Journal, 224 (1978) 241–246.
22. **Vernazza J.E.**, **Avrett E.H.**, **Loeser R.**, Structure of the solar chromosphere. III - Models of the EUV brightness components of the quiet-sun, The Astrophysical Journal Supplement Series, 45 (1981) 635–725.
23. **Masuda S.**, **Kosugi T.**, **Hara H.**, **Tsuneta S.**, **Ogawara Y.**, A loop-top hard X-ray source in a compact solar flare as evidence for magnetic reconnection, Nature, 371 (1994) 495–497.

24. **Mariska J.T.**, **Emslie A.G.**, **Li P.**, Numerical simulations of impulsively heated solar flares, The Astrophysical Journal, 341 (1989) 1067–1074.

25. **Melnikov V.F.**, **Reznikova V.E.**, **Shibasaki K.**, **Nakariakov V.M.**, Spatially resolved microwave pulsations of a flare loop, Astronomy & Astrophysics, 439 (2) (2005) 727–736.

26. **Reznikova V.E.**, **Melnikov V.F.**, **Shibasaki K.**, **Gorbikov S.P.**, **Pyatakov N.P.**, **Myagkova I.N.**, **Ji H.**, 2002 august 24 limb flare loop: dynamics of microwave brightness distribution, The Astrophysical Journal, 697 (1) (2009) 735–746.

27. **Shabalin A.N.**, **Ovchinnikova E.P.**, **Globina V.I.**, **Charikov Y.E.**, Accelerated Electron Propagation Model for the Flare Arcade of the September 23, 2014, Event from RHESSI, SDO, and Nobeyama Radioheliograph Observations, Geomagnetism and Aeronomy, 59 (8) (2019) 1128–1138.

THE AUTHORS

SHABALIN Alexander N.
ShabalinAN@mail.ioffe.ru
ORCID: 0000-0003-3938-0146

CHARIKOV Yuri E.
Yuri.Charikov@mail.ioffe.ru
ORCID: 0000-0002-6693-5613

Received 29.10.2022. Approved after reviewing 08.11.2022. Accepted 08.11.2022.